ADVANCED FUNCTIONAL MATERIALS
www.afm-journal.de

Novel Nanoscale Twinned Phases in Perovskite Oxides

Sergey Prosandeev, Dawei Wang, Wei Ren, Jorge Íñiguez, and Laurent Bellaiche*

Perovskite oxides form a fascinating class of materials because they possess many active degrees of freedom that result in a large variety of physical effects. One important structural parameter controlling the behavior of perovskites is the tilting of the oxygen octahedral. Among other properties, this tilting is coupled with the electric and magnetic orders, which leads to novel and potentially useful phenomena; recent examples include new mechanisms for improper and triggered ferroelectricity, rich phase diagrams, and novel chiral phases, counter-intuitive behaviors of ferroelectric and multiferroic films, and weak ferromagnetism in otherwise antiferromagnetic materials. Interestingly, most perovskites present the same tilted structures, which are few in number and fairly simple. In contrast, here we use different theoretical methods to show that a complete new family of stable phases, all displaying complex and nano-twinned tilting patterns (as well as other anomalous properties), exists in multiferroic $BiFeO_3$ and related compounds.

1. Introduction

The antiferrodistortive (AFD) mode, which corresponds to the tilting of the oxygen octahedral, is a fundamental and important structural degree of freedom of perovskite oxides.[1–18] The two most common types of oxygen-octahedra tiltings are antiphase (associated with the *R* point of the 5-atom cubic first Brillouin zone) and in-phase (associated with the *M* point).[8,9] The first type corresponds to a periodic pm pattern, where one O_6 octahedron rotates clockwise (sign of the rotation is plus or p) about a <001> pseudo-cubic direction and the neighboring octahedron along the same <001> direction rotates counterclockwise (minus or m) about the same axis. The second type corresponds to a periodic pp or mm pattern. In very few bulks, such as $NaNbO_3$, $AgNbO_3$ and $(Ca,Sr)TiO_3$,[19–23] the octahedra tiltings adopt an alternative arrangement: namely, the ppmm periodic pattern, which can be viewed as series of nanoscale twinned octahedral tiltings. This AFD pattern was also suggested to induce unusual antiferroelectricity, where the associated k-point is not at the zone boundary but rather in-between the Γ and *X* points.[23]

In light of such facts, and in order to gain an even deeper knowledge of perovskites, interesting questions are: May other and more complex tilting patterns, with even longer periods (e.g., pppmmm, ppmppm, ppppmm, pppppm, be awaiting to be discovered? If yes, what bulk material(s) can present them, what are the physical requirements for such nano-twinned patterns to exist, and are they coupled with other structural degrees of freedom?

Here, we provide answers to these questions. In particular, we report the prediction of a complete family of phases with complex, nanoscale twinned-AFD patterns in one of the most currently studied materials, room-temperature multiferroic $BiFeO_3$ (BFO). Such unusual phases have very similar low energy. They also exhibit a non-vanishing spontaneous polarization as well as anomalous antiferroelectric displacements (that are associated with k-points that are not located at the zone boundary), which therefore reveals novel couplings between long-range ordered electric dipoles and AFD distortions. Our simulations further suggest that these phases act as structural bridges between the known *R*3*c* and *Pnma* states when varying some physical quantity, such as temperature and pressure in BFO or composition in $(Bi,R)FeO_3$ solid solutions where R is a rare-earth atom. Therefore, in addition to providing novel condensed-matter phases, this study also leads to a revisiting of BFO and related-materials.

2. Results and Discussion

The discovery of these nano-twinned tilting patterns occurred as a result of our efforts to generalize the effective Hamiltonian of ref. [18,24,25] in order to include terms that can lead to the appearance of the *Pnma* phase as a (meta)stable state. For that, the degrees of freedom were chosen to be 1) the local soft mode in unit cell *i*, $\mathbf{u}_i$, which is directly proportional to the electrical dipole centered on that site. These local modes are centered on

Dr. S. Prosandeev, Dr. W. Ren, Prof. L. Bellaiche
Physics Department and Institute for Nanoscience and Engineering
University of Arkansas
Fayetteville, AR 72701, USA
E-mail: sprossan@uark.edu
Dr. D. Wang
Electronic Materials Research Laboratory
Key Laboratory of the Ministry of Education and International Center for Dielectric Research
Xi'an Jiaotong University
Xi'an 710049, China
Dr. W. Ren
Department of Physics
Shanghai University
99 Shangda Road, Shanghai 200444, China
Dr. J. Íñiguez
Institut de Ciència de Materials de Barcelona (ICMAB-CSIC)
Campus UAB, 08193 Bellaterra, Spain

DOI: 10.1002/adfm.201201467

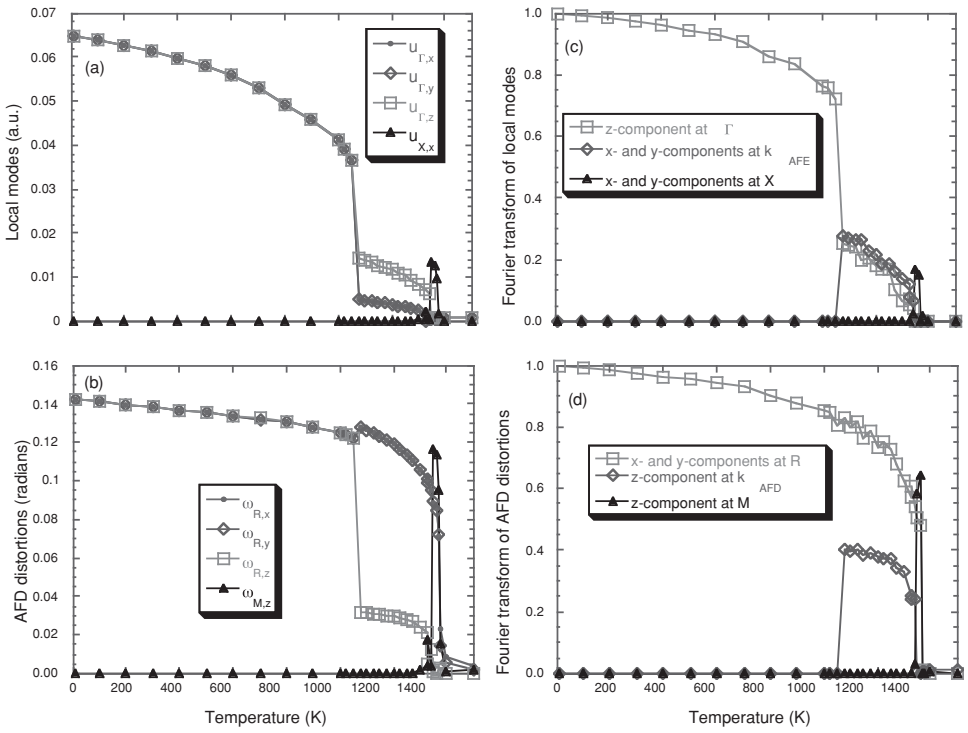

Figure 1. Temperature dependency of different properties in $BiFeO_3$ bulk, as predicted by the present effective Hamiltonian. a) The Cartesian components of the $\mathbf{u}_\Gamma$ supercell average of the local mode vectors and the x-component (which is also equal to its y-component) of the $\mathbf{u}_X$ vector characterizing antiferroelectricity at the X-point. b) The Cartesian components of the ω_R vector representing antiphase tilting of the oxygen octahedra, as well as the z-component of the ω_M vector that quantifies in-phase oxygen octahedral tilting. c) The square of the Fourier transforms of some selected Cartesian components of the local modes' configuration at the Γ, *X* and $\mathbf{k}_{AFE}$ points (see text). d) Similar information but for the AFD distortions at the *R*, *M* and $\mathbf{k}_{AFD}$ points (see text).

Bi sites here, which allows for the antiferroelectricity found in BFO[26] to occur and which contrasts with the approaches of ref. [18,24,25]; 2) the homogeneous and inhomogeneous strain tensors;[27] 3) the (Fe-centered) pseudo-vectors, $\{\omega_i\}$, that characterize the direction and magnitude of the AFD distortions in unit cell *i*;[13] and 4) the magnetic dipole moments centered on the Fe-sites. Details about the analytical expression of the total energy, E_{tot}, of this novel effective Hamiltonian are given in the Methods Section. As in ref. [18,24,25], all the parameters involved in E_{tot} were determined by performing local-density-approximation (LDA) calculations with a Hubbard-*U* correction,[28] adopting the value of 3.8 eV for *U*; E_{tot} is then used in Monte-Carlo (MC) simulations to compute finite-temperature properties of $BiFeO_3$. These MC simulations yield a (meta)stable *Pnma* state that has a energy that lies 33 meV/5-atom above the *R3c* ground state. This prediction is consistent with the fact that density functional theory calculations provided a corresponding energy ranging between 14 and 60 meV/5-atom, depending on the functional used.[26] Furthermore, we also decided to apply a negative pressure of −6 GPa in the MC computations, in order to correct for the underestimation of the theoretical LDA lattice constant (note that, under such pressure condition, the presently described effective Hamiltonian method yields a *Pnma* state lying 70 meV/5-atom above the *R3c* ground state). Outputs of the MC simulations that are relevant to the present study are: 1) the $\mathbf{u}_\Gamma$ supercell average of the local mode vectors $\{\mathbf{u}_i\}$, which is directly proportional to the electric polarization. 2) The ω_R vector that represents antiphase-tilting of the oxygen octahedra and that is defined as $\omega_R = \frac{1}{N}\sum_i \omega_i(-1)^{n_x(i)+n_y(i)+n_z(i)}$, where the sum runs over the *N* sites *i* and $n_x(i)$, $n_y(i)$ and $n_z(i)$ are integers locating the cell *i*.[13] More precisely, in the ideal perovskite structure, and denoting the 5-atom cubic lattice constant by a_{lat}, this cell *i* is centered at $a_{lat}(n_x(i)\mathbf{x} + n_y(i)\mathbf{y} + n_z(i)\mathbf{z})$ with respect to a chosen origin, with **x**, **y** and **z** being unit vectors along the [100], [010] and [001] pseudo-cubic directions, respectively. 3) the $\mathbf{u}_X$ vector that characterizes antiferroelectricity at the X-point, and that is given by $\mathbf{u}_X = \frac{1}{N}\sum_i \mathbf{u}_i(-1)^{n_z(i)}$. 4) The ω_M vector that quantifies in-phase oxygen octahedral tilting and that is provided by $\omega_M = \frac{1}{N}\sum_i \omega_i(-1)^{n_x(i)+n_y(i)}$.

All these quantities are shown in **Figure 1**, when choosing a 12 × 12 × 12 supercell (8640 atoms) to mimick BFO bulks and using 40 000 MC sweeps with this novel effective Hamiltonian scheme to get well-converged results. We start from the *R3c* ground state at 10K and progressively increase the temperature. Figure 1a,b show that our approach predicts that the *R3c* state persists up to $T_c \approx 1075$K (this *R3c* state is characterized by a polarization pointing along the [111] direction, as indicated by $u_{\Gamma,x} = u_{\Gamma,y} = u_{\Gamma,z} \neq 0$, and by oxygen octahedra tilting in antiphase fashion about the same [111] direction, as characterized by $\omega_{R,x} = \omega_{R,y} = \omega_{R,z} \neq 0$). BFO bulk then undergoes

a first-order transition just above this critical temperature, as consistent with measurements (see ref. [29–32] and references therein) and as evidenced by the jump in both $\mathbf{u}_\Gamma$ and ω_R. However, the resulting phase is not the *Pnma* state that has been proposed based on neutron diffraction,[31] since it possesses neither antiferroelectricity associated with the *X*-point nor in-phase tilting. In fact, Figure 1a,b further reveal that the *Pnma* state "only" appears at higher temperatures, specifically between 1325 K and 1375 K here (above this latter temperature, the system becomes cubic; note that the melting point of BFO is around 1240 K,[24] which therefore may prevent the observation of the high-temperature *Pnma* state). In other words, a "mysterious" phase exists in a relatively large temperature window between the known *R3c* and *Pnma* states of BFO. Surprisingly, this previously unknown phase is polar, with a polarization pointing along a [*uuv*] direction with *v* larger than *u* (see Figure 1a), which makes it monoclinic rather than orthorhombic. Interestingly, ref. [30] indeed proposed that the phase experimentally seen just above T_c in pure BFO has a monoclinic symmetry. However, the authors of this study did not consider the possibility that this phase could also display a spontaneous polarization. Figure 1b further indicates that this phase also exhibits large anti-phase tilting of the oxygen octahedra about [110] superimposed on a much smaller $\omega_{R,z}$. To better characterize this structure, we computed the Fourier transforms (FT) of the $\{u_i\}$ and $\{\omega_i\}$ configurations, at all investigated temperatures, for the different reciprocal k-points compatible with our $12 \times 12 \times 12$ supercell.[33] The results are displayed in Figure 1c,d for the Cartesian components of the local modes and AFD distortions, respectively, for some representative k-points. The mysterious phase possesses a significant FT of the *z*-component of the local mode at Γ (as consistent with the existence of the *z*-component of the polarization) and a large FT of the *x*- and *y*-components of the AFD distortions at the *R*-point of the cubic Brillouin zone (as representative of its anti-phase tilting of the oxygen octahedra about [110]). This phase also exhibits a large FT component of the *z*-component of the $\{\omega_i\}$'s at $\mathbf{k}_{\mathrm{AFD}} = \frac{2\pi}{a_{lat}}(\frac{1}{2}\mathbf{x} + \frac{1}{2}\mathbf{y} + \frac{1}{6}\mathbf{z})$. This k-point is located in-between the *R* and *M* points of the cubic Brillouin zone, and characterizes unusual pattern for the *z*-component of the AFD motion when moving along a line joining Fe ions along the [001] direction: following such a line provides a pppmmm periodic pattern for this z-component, where p and m denote a tilting about [001] and $[00\bar{1}]$, respectively (*R3c* and *Pnma* states yield periodic pm and pp patterns, respectively, for this *z*-component). In other words, adopting a modified Glazer notation,[8] the whole AFD configuration would be given by (a^- a^- "complex"), where "complex" refers to the pppmmm periodic pattern (it is straighforward to prove that a pppmmm pattern along [001] yields a vanishing *z*-component of the ω_M quantity but results in a non-zero z-component of the ω_R vector). The resulting phase can thus been seen as a nanoscale twinned octahedral tilting pattern with a relatively long period, namely 6 lattice constants along [001]. Interestingly, ref. [34] indicates that a similar phase, which may present an inhomogeneous pattern for the *z*-component of the AFD distortions that would be associated with a k-point that is neither *R* nor *M*, in addition to possessing anti-phase oxygen octahedral tilting about [110], may occur in $Bi_{1-x}R_xFeO_3$ solid solutions where R is rare-earth element. As a matter of fact, nanoscale twinned octahedral tilting patterns could explain the mysterious phase experimentally detected[35–38] in a narrow compositional region bridging the morphotropic transition between the *R3c* (small *R* content) and *Pnma* (large *R* content) phases, where large physical responses have been reported.[36] Indeed, such an explanation seems much simpler and much more natural than the recently proposed notion[38] that modulated phases controlled by flexoelectric interactions occur in that region of the phase diagram. Increasing the temperature in pure BFO thus appears to have the same effect than increasing the rare-earth composition in $Bi_{1-x}R_xFeO_3$ solid solutions at room temperature, that is, to create a complex tilting phase in-between the known *R3c* and *Pnma* states. Furthermore, the presently discovered peculiar AFD pattern is also accompanied by antiferroelectric Bi-displacements that are either directed along [110] or $[\bar{1}\bar{1}0]$, depending on the (001) Bi-plane. Such displacements are associated with a k-point that is not at the zone boundary of the cubic Brillouin zone (unlike in the Pnma state). Rather and as indicated by Figure 1c, this latter k-point is given here by $\mathbf{k}_{\mathrm{AFE}} = \frac{2\pi}{3a_{lat}}\mathbf{z}$, and is therefore located in-between the Γ and *X* points.

We also varied the size of the supercells used in the MC simulations, and always found a temperature regime for which a complex phase possessing a nano-twinned octahedral tilting pattern and unusual antiferroelectric displacements exists between the *R3c* and *Pnma* states. All these intermediate phases possess anti-phase tilting about [110], and a polarization having a significant *z*-component but not necessarily having *x*- and *y*-components. As a result, these intermediate phases can also be of orthorhombic symmetry, i.e., they are not always monoclinic. Such a feature may be consistent with the fact that a ferroelectric orthorhombic phase has once been proposed to exist above $T_c \approx 1100$ K in pure BFO.[32] Interestingly, the $\mathbf{k}_{\mathrm{AFD}}$ vector characterizing such complex phases can vary, implying that the kind of periodic pattern for the *z*-component of the AFD can change. For instance, we also found ppmppm, ppppmm and ppmm patterns, for which the antiferroelectricity is associated with $\mathbf{k}_{\mathrm{AFE}} = \frac{2\pi}{6a_{lat}}\mathbf{z}$, $\frac{2\pi}{6a_{lat}}\mathbf{z}$ and $\frac{2\pi}{4a_{lat}}\mathbf{z}$, respectively. Note that our predictions are fully consistent with the suggestion in ref. [23] that the twinned AFD (ppmm) structure of $(Ca,Sr)TiO_3$ induces unusual antiferroelectricity (with $\mathbf{k}_{\mathrm{AFE}}$ lying between Γ and *X*), and also with the experimental finding that the complex oxygen octahedral tilting pattern of $AgNbO_3$ (which is also ppmm) possesses a spontaneous polarization along [001]. Further, our results indicate that a complete family of nanoscale twinned-tilting phases, characterized by nearly-arbitrary O_6-rotation sequences and long repetition periods, can exist in BFO and related materials! It is also important to know that the amplitudes of the p and m tilts, or even the amplitudes of different p (or m) tilts, do not need to coincide within these nano-twinned phases, and that we did not find any low-energy structure for which some of these tilts are vanishing.

One way to understand why BFO possesses various, quasi-degenerate twinned octahedral tilting structures is as follows. Let us first focus on the sole interaction between two oxygen octahedra for which the respective Fe centers are nearest neighbors of each other along [001]. The sign of the AFD parameter controlling such interaction is slightly positive in BFO, implying that the *z*-components of the AFDs prefer to be in

antiphase rather than in-phase. Moreover, antiphase AFD instabilities are accompanied by the formation of a spontaneous polarization because of the fourth term of Equation (1) given in the Methods Section, which is consistent with the occurrence of the *R*3*c* phase as the ground state of BFO. However, the sixth term of that Equation (1) implies that in-phase AFD instabilities along the *z*-axis can also have their energy considerably decreased when both antiferroelectricity and antiphase tilting occur along the in-plane [110] direction, which is consistent with the fact that Pnma is also a (meta)stable state of BFO. These competing interactions (that is anti-phase tilting accompanied by ferroelectricity versus out-of-plane in-phase tilting accompanied by both in-plane anti-phase tilting and antiferroelecticity) lead to a frustration in BFO and related materials. Such a frustration is the mechanism responsible for the occurrence of the nanoscale twinned octahedral tilting structures, since they possess *all* the aforementioned competing interactions active. This frustration also explains why these nano-twinned structures act as a bridge between the *R*3*c* and *Pnma* states, which are the limiting cases in which one of the competing structural variants prevails over the other. Frustration is also likely to be the mechanism responsible for the ppmm patterns experimentally found in $NaNbO_3$, $AgNbO_3$ and $(Ca,Sr)TiO_3$.[19–23] Moreover, the fact that *R*3*c* and *Pnma* are known to both occur in various families of perovskite materials strongly suggests that the nanoscale twinned octahedral tilting structures that we have discovered will be found (or induced) in other compounds in a near future.

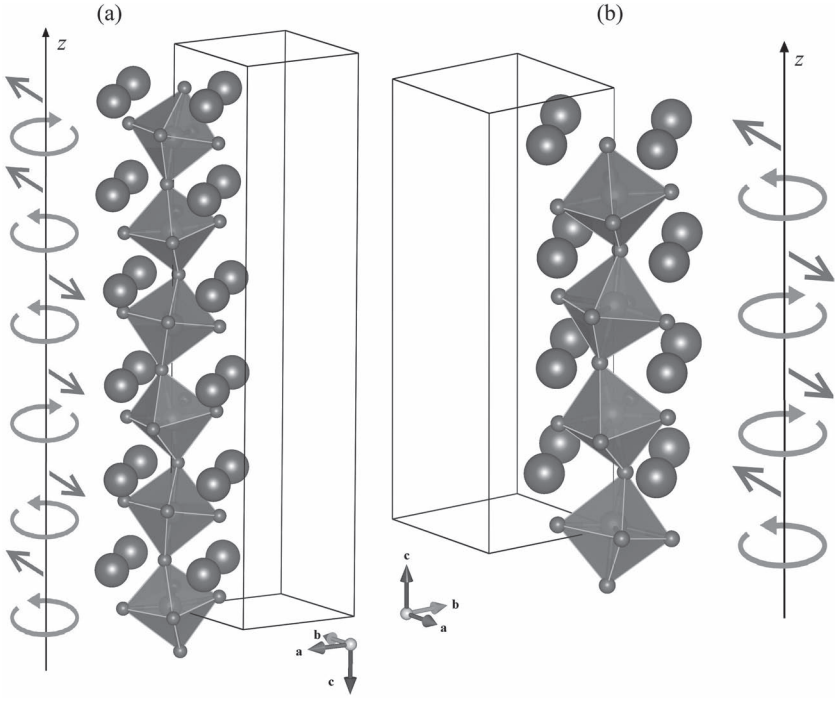

Figure 2. Schematic of the nanoscale twinned octahedral tilting structures found by first-principle calculations. a,b) The ppmppm and ppmm patterns, respectively. The straight arrows represent the antiferroelectric Bi displacements (that are oriented along the [110] or [$\bar{1}\bar{1}$0] pseudo-cubic directions), while the curled arrows indicate if the displayed oxygen octahedral tilting is counterclockwise or clockwise.

To test the provocative results arising from our new effective Hamiltonian (Heff) for BFO, we performed direct first-principles calculations. Technical details are reported in the Methods Section. These $T = 0$ K *ab initio* simulations indeed resulted in a variety of stable twinned octahedral tilting phases. Interestingly, their energies are all lower than that of the *Pnma* structure, but higher than that of the *R*3*c* ground state. For instance, the complex phases displayed in **Figure 2**, which correspond to the "ppmppm" and "ppmm" patterns for the *z*-component of the AFD distortions, have an energy lying only 23 meV/5-atom and 32 meV/5-atom, respectively, above the *R*3*c* state, to be compared with the corresponding value of 60 meV/5-atom for the *Pnma* structure. These ppmppm and ppmm patterns are found to adopt the orthorhombic $Pna2_1$ and $Pca2_1$ space groups, respectively. Our first-principles calculations also confirmed other predictions of the Heff approach, namely, the occurrence of a polarization having a significant *z*-component, an antiphase octahedral tilting about [110], and antiferroelectric displacements of Bi atoms along [110] or [$\bar{1}\bar{1}$0] that are associated with k-points that do not lie at the zone boundary (see Figure 2).

One may also wonder if, in addition to increasing the temperature in pure BFO and varying the composition in $(Bi,R)FeO_3$ systems, there is another way to detect these nano-twinned phases. We think there are good reasons to believe that the "mysterious" structures seen in BFO under pressure (once again, occurring in-between the *R*3*c* and *Pnma* states), and for which different space groups have been proposed (see ref. [39,40,41] and references therein), are in fact instances of such phases. This belief is supported by the results in **Figure 3**, which reports the volume variation of different phases as a function of pressure in pure BFO, as measured in ref. [39] and as computed from our first-principles simulations. For low-pressure, the calculations reproduce very well the experimentally observed decrease of the volume of the *R*3*c* ground state. Similarly, for pressure above 11 GPa, the measured *Pnma* state has its volume variation well mimicked by first principles. The most striking feature of Figure 3 is that the "mysterious" phase experimentally seen by various groups has a pressure-induced volume variation that perfectly matches the first-principles results for some of our discovered nanoscale twinned octahedral tilting phases (in this case, those corresponding to the pppmm and pppppm patterns, which both adopt a monoclinic *Pc* space group). Such a perfect match strongly suggests that the intermediate phase experimentally detected indeed presents the predicted nano-twinned octahedral tiltings with a longer than usual period. We note, however, that first-principles calculations indicate that the nanoscale twinned octahedral tilting phases are never the ground state with increasing pressure. In other words, the computed enthalpies of the phases mentioned in Figure 3 yield a direct first-order transition from *R*3*c* to *Pnma* under compression. This difference with the measurements

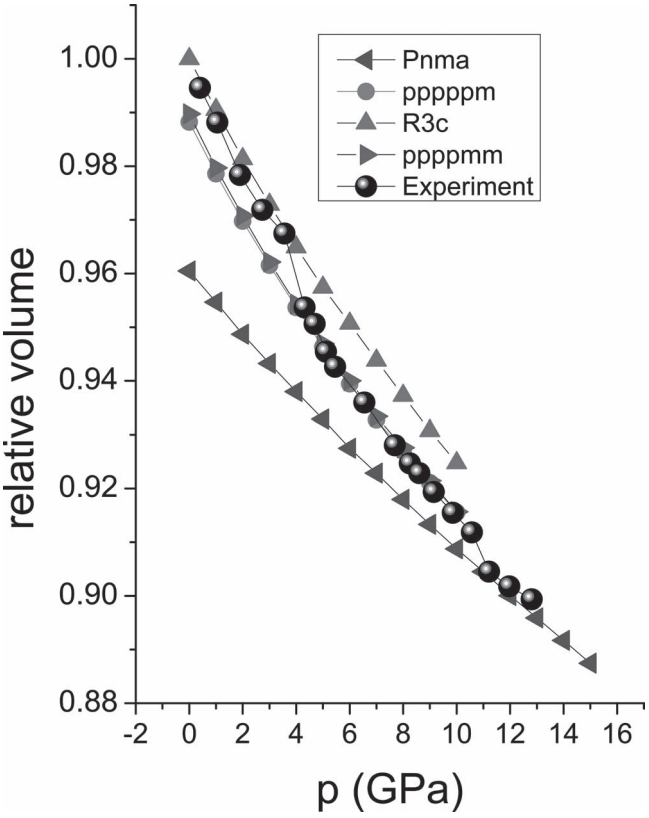

Figure 3. Pressure dependency of the relative volume (with respect to that of the *R3c* ground state at zero pressure) of some selected phases, as predicted by our first-principle calculations. The experimental data of ref. [39] are provided for comparison.

likely arises either from the fact that kinetics play an important role in determining the intermediate phases experimentally seen, or from the fact that our first-principles calculations were performed at T = 0 K while the measurements were done at room temperature (note that, according to Figure 1, increasing the temperature brings the nano-twinned octahedral tilting structures closer to the *R3c* state in free energy).

3. Conclusions

In conclusion, our results show that $BiFeO_3$ and related materials can present a family of quasi-degenerate phases that display nanoscale twinned octahedral-tilting patterns. On top of answering several important open questions concerning these multiferroic compounds, our work also reveals the physical origins of these patterns and their coupling with polarization and unusual antipolar displacements. It is also interesting to realize that a very recent work[42] experimentally found nano-twinned oxygen octahedral tilting structures having a period of four and six lattice constants (i.e., exactly as in the present study) in another compound, namely $NaNbO_3$. Such finding, combined with our present predictions, implies that complex AFD patterns likely exist in a variety of materials.[43] We thus hope our study will be of large benefit to researchers working on perovskites, and of broad interest to the materials science community.

4. Methods Section

Effective Hamiltonian: Its degrees of freedom are 1) the local soft mode in unit cell i, $\mathbf{u}_i$, which are centered on Bi sites here and therefore allows for the antiferroelectricity found in BFO systems[26] to be able to occur; 2) the homogeneous and inhomogeneous strain tensors,[27] to be denoted by $\{\eta_H\}$ and $\{\eta_I\}$, respectively; 3) the (Fe-centered) pseudo-vectors, $\{\omega_i\}$, that characterize the direction and magnitude of the AFD distortions in unit cell i[13]; and 4) the magnetic dipole moments, $\mathbf{m}_i$, centered on the Fe-sites i–with the magnitude of these moments being equal to 4 μB, as consistent with first principles[44] and measurements.[45] The total energy, E_{tot}, of this Hamiltonian is written as a sum of three main terms: (i) $E_1(\{u_i\}, \{\eta_H\}, \{\eta_I\})$, which represents the energy associated with local modes, elastic interactions, and the coupling between local modes and strains; (ii) $E_2(\{\mathbf{m}_i\}, \{\mathbf{u}_i\}, \{\eta_H\}, \{\eta_I\}, \{\omega_i\})$, which gathers the energies involving the magnetic degrees of freedom and their interactions with local modes, AFD distortions and strains; and (iii) $E_3(\{\mathbf{u}_i\}, \{\eta_H\}, \{\eta_I\}, \{\omega_i\})$, which characterizes the AFD interactions and their couplings with local modes and strains. The analytical expressions of E_1 and E_2 are provided in ref. [27,18], respectively, while we propose here the following expression for E_3:

$$
\begin{aligned}
E_3(\{\mathbf{u}_i\}, \{\eta_H\}, \{\eta_I\}, \{\omega_i\}) = & \sum_i \left[\kappa_A \omega_i^2 + \alpha_A \omega_i^4 \right. \\
& \left. + \gamma_A \left(\omega_{i,x}^2 \omega_{i,y}^2 + \omega_{1ti,y}^2 \omega_{i,z}^2 + \omega_{i,x}^2 \omega_{i,z}^2\right)\right] \\
& + \sum_{i,j} \sum_{\alpha,\beta} K_{ij,\alpha\beta} \omega_{i,\alpha} \omega_{j,\beta} \\
& + \sum_i \sum_{\alpha,\beta} C_{l,\alpha\beta} \eta_l(i) \omega_{i,\alpha} \omega_{i,\beta} \\
& + \sum_{i,j} \sum_{\alpha,\beta,\gamma,\delta} D_{\alpha\beta\gamma\delta} \omega_{i,\alpha} \omega_{i,\beta} u_{j,\gamma} u_{j,\delta} \\
& + \sum_{i,j} \sum_{\alpha} K'_{ij} \omega_{i,\alpha}^3 \omega_{j,\alpha} \\
& + \sum_{i,j} \sum_{\alpha,\beta} D'_{ij,\alpha\beta} \omega_{i,\alpha} \omega_{i,\beta} u_{j,\alpha}
\end{aligned}
\tag{1}
$$

where the sums over i run over all Fe-sites. j runs over the six Fe atoms that are nearest neighbors (in the Fe-sublattice) of the Fe-site i in the second and fifth energies, while it runs over the eight Bi atoms that are nearest neighbors of that Fe-site i in the fourth and sixth energetic terms. $\eta_l(i)$ is the l^{th} component of the total strain at the site i. α, β, γ and δ denote Cartesian components, with the x-, y- and z-axes being along the pseudo-cubic [100], [010] and [001] directions, respectively. The first four energies have been previously proposed and/or used in ref. [13,18,24,25]. They correspond to the self-energy associated with AFD distortions, the harmonic short-range energy between

AFD degrees of freedom, the interaction energy between strain and ω_i, and the harmonic interaction energy between local-modes and AFD motions, respectively. The novelty of the present approach with respect to ref. [13,18,24,25] resides in the fifth and sixth terms of Equation (1), which represent anharmonic short-range energy between AFD distortions and an interaction energy between local modes and AFD motions that is harmonic in ω_i while being linear in $\mathbf{u}_i$, respectively. It was numerically found that 1) the fifth energy allows phases, such as *Pnma*, exhibiting a coexistence of antiphase (about some axes) and in-phase (about perpendicular axes) oxygen octahedra tilting to occur and 2) the sixth energy activates the antiferroelectric Bi displacements that are also inherent to *Pnma*.[26]

First-Principles Computations: The Perdew-Burke-Ernzerhof (PBE) generalized gradient approximation (GGA),[46] as implemented in the VASP package,[47] was used. This functional has been shown to be the most appropriate one to study the relative stability of $BiFeO_3$'s *R*3*c* and *Pnma* phases.[26] A Hubbard-*U* correction[28] was employed for a better treatment of Fe 3*d* electrons. The *U* parameter was chosen to be 3.87 eV, as in ref. [24]. The projected augmented wave (PAW) method[48] was adapted to represent the ionic cores, solving for the following valence electrons: Fe 3*p*, 3*d* and 4*s*; Bi 5*d*, 6*s* and 6*p*; and O 2*s* and 2*p*. A plane-wave basis was used and truncated at 500 eV, and a $4 \times 4 \times 1$ *k*-point mesh was used for integrations within the first Brillouin zone. Different supercells, all adopting a *G*-type antiferromagnetic order, were constructed. They all have the basic lattice vectors (expressed in the pseudo-cubic setting): $a_{lat}(u, -u, 0)$, $a_{lat}(v,v, 0)$, and $a_{lat}(0, 0, nw)$, where a_{lat} is the lattice parameter, while *u*, *v*, and *w* are variables with values very close to 1 and *n* is the number of the FeO_2 layers stacked along the [001] direction. Practically, $n = 4$ and $n = 6$ were used. Note that a_{lat}, *u*, *v*, and *w* were all relaxed to minimize the total energy and the calculations were chosen to be converged when all forces were less than 0.001 eV/Å. Furthermore, for the calculations corresponding to Figure 3 of the manuscript and associated with the hydrostatic pressure, *P*, the enthalpy $H = E + PV$, was computed, where *E* is the total internal energy and *V* is the volume, as implemented in the VASP package.[47]

Acknowledgements

The authors thank M. Guennou, P. Bouvier, I. Levin, P. Lightfoot, and M. Glazer for useful discussions. This work was mostly financially supported by ONR Grants N00014-11-1-0384 and N00014-08-1-0915, and ARO Grant W911NF-12-1-0085. The authors also acknowledge Department of Energy, Office of Basic Energy Sciences, under contract ER-46612 and the NSF grants DMR-1066158 and DMR-0701558 for discussions with scientists sponsored by these grants. D.W. acknowledges support from the National Natural Science Foundation of China under Grant No. 10904122. W.R. acknowledges the Eastern Scholar Professorship at Shanghai Institutions of Higher Education, Shanghai Municipal Education Commission. J.I. acknowledges funding from MINECO-Spain (Grants Nos. MAT2010-18113, MAT2010-10093-E and CSD2007-00041). Some computations were also made possible thanks to the MRI grant 0722625 from NSF, the ONR grant N00014-07-1-0825 (DURIP) and a Challenge grant from the Department of Defense.

Received: June 1, 2012
Revised: July 10, 2012
Published online: August 24, 2012

[1] G. Catalan, J. F. Scott, *Adv. Mater.* **2009**, *21*, 2463.
[2] O. Auciello, J. F. Scott, R. Ramesh, *Phys. Today* **1998**, *51*, No. 7, 22.
[3] M. E. Lines, A. M. Glass, *Principles and Applications of Ferroelectrics and Related Materials*, Clarendon Press, Oxford **1977**.
[4] S.-W. Cheong, M. Mostovoy, *Nat. Mater.* **2007**, *6*, 13.
[5] R. Ramesh, N. A. Spaldin, *Nat. Mater.* **2007**, *6*, 21.
[6] B. Keimer, *Nat. Mater.* **2006**, *5*, 9333.
[7] R. J. Cava, B. Batlogg, J. J. Krajewski, R. Farrow, L. W. Rupp, Jr, A. E. White, K. Short, W. F. Peck, T. Kometani, *Nature* **1998**, *332*, 814.
[8] A. M. Glazer, *Acta Crystallogr. Sect. A* **1975**, *31*, 756.
[9] a) H. T. Stokes, E. H. Kisi, D. M. Hatch, C. J. Howard, *Acta Cryst. B* **2002**, *58*, 934; b) C. J. Howard, H. T. Stokes, *Acta Cryst. B* **1998**, *54*, 782.
[10] E. Bousquet, M. Dawber, N. Stucki, C. Lichtensteiger, P. Hermet, S. Gariglio, J.-M. Triscone, P. Ghosez, *Nature* **2008**, *452*, 732.
[11] I. A. Kornev, L. Bellaiche, *Phys. Rev. B* **2009**, *79*, 100105.
[12] N. A. Benedek, C. J. Fennie, *Phys. Rev. Lett.* **2011**, *106*, 107204.
[13] I. A. Kornev, L. Bellaiche, P. E. Janolin, B. Dkhil, E. Suard, *Phys. Rev. Lett.* **2006**, *97*, 157601.
[14] D. Sichuga, W. Ren, S. Prosandeev, L. Bellaiche, *Phys. Rev. Lett.* **2010**, *104*, 207603.
[15] D. Sichuga, I. Ponomareva, L. Bellaiche, *Phys. Rev. B* **2009**, *80*, 134116.
[16] I. C. Infante, S. Lisenkov, B. Dupe, M. Bibes, S. Fusil, E. Jacquet, G. Geneste, S. Petit, A. Courtial, J. Juraszek, L. Bellaiche, A. Barthelemy, B. Dkhil, *Phys. Rev. Lett.* **2010**, *105*, 057601.
[17] C. Ederer, N. A. Spaldin, *Phys. Rev. B* **2005**, *71*, 060401.
[18] D. Albrecht, S. Lisenkov, Wei Ren, D. Rahmedov, Igor A. Kornev, L. Bellaiche, *Phys. Rev. B* **2010**, *81*, 140401.
[19] V. A. Shuvaeva, M. Y. Antipin, S. V. Lindeman, O. E. Fesenko, V. G. Smotrakov, Y. T. Struchkov, *Sov. Phys. Crystallogr.* **1992**, *37*, 814.
[20] S. L. Samal, G. K. Pradhan, C. Narayana, A. K. Ganguli, *Solid State Sci.* **2009**, *11*, 562.
[21] K. E. Johnston, C. C. Tang, J. E. Parker, K. S. Knight, P. Lightfoot, S. E. Ashbrook, *J. Am. Chem. Soc.* **2010**, *132*, 8732.
[22] M. Yashima, S. Matsuyama, R. Sano, M. Itoh, K. Tsuda, D. Fu, *Chem. Mater.* **2011**, *23*, 1643.
[23] C. J. Howard, R. L. Withers, K. S. Knight, Z. Zhang, *J. Phys.: Condens. Matter* **2008**, *20*, 135202.
[24] I. A. Kornev, S. Lisenkov, R. Haumont, B. Dkhil, L. Bellaiche, *Phys. Rev. Lett.* **2007**, *99*, 227602.
[25] a) S. Lisenkov, Igor A. Kornev, L. Bellaiche, *Phys. Rev. B* **2009**, *79*, 012101; b) S. Lisenkov, Igor A. Kornev, L. Bellaiche, *Phys. Rev. B* **2009**, *79*, 219902.
[26] O. Diéguez, O. E. González-Vázquez, Jacek C. Wojdeł, Jorge Iñiguez, *Phys. Rev. B* **2011**, *83*, 094105.
[27] a) W. Zhong, D. Vanderbilt, K. M. Rabe, *Phys. Rev. Lett.* **1994**, *73*, 1861; b) W. Zhong, D. Vanderbilt, K. M. Rabe, *Phys. Rev. B* **1995**, *52*, 6301.
[28] V. I. Anisimov, F. Aryasetiawan, A. I. Lichtenstein, *J. Phys: Condens. Matter* **1997**, *9*, 767.
[29] R. Haumont, J. Kreisel, P. Bouvier, F. Hippert, *Phys. Rev. B* **2006**, *73*, 132101.
[30] R. Haumont, Igor A. Kornev, S. Lisenkov, L. Bellaiche, J. Kreisel, B. Dkhil, *Phys. Rev. B* **2008**, *78*, 134108.
[31] D. C. Arnold, K. S. Knight, F. D. Morrison, P. Lightfoot, *Phys. Rev. Lett.* **2009**, *102*, 027602.
[32] R. Palai, R. S. Katiyar, J. F. Scott, *Cond-mat* **2007**, 0705.2883v1.
[33] A. M. George, J. Iñiguez, L. Bellaiche, *Phys. Rev. B* **2002**, *65*, 180301.
[34] I. Levin, M. G. Tucker, H. Wu, V. Provenzano, C. L. Dennis, S. Karimi, T. Comyn, T. Stevenson, R. I. Smith, I. M. Reaney, *Chem. Mater.* **2011**, *23*, 2166.
[35] S. B. Emery, C.-J. Cheng, D. Kan, F. J. Rueckert, S. P. Alpay, V. Nagarajan, I. Takeuchi, B. O. Wells, *Appl. Phys. Lett.* **2010**, *97*, 152902.

[36] D. Kan, L. Palova, V. Anbusathaiah, C. J. Cheng, S. Fujino, V. Nagarajan, K. M. Rabe, I. Takeuchi, *Adv. Funct. Mater.* **2010**, *20*, 1108.
[37] I. Levin, S. Karimi, V. Provenzano, C. Dennis, H. Wu, T. Comyn, T. Stevenson, R. I. Smith, I. M. Reaney, *Phys. Rev. B* **2010**, *81*, 020103.
[38] A. Y. Borisevich, E. A. Eliseev, A. N. Morozovska, C.-J. Cheng, J.-Y. Lin, Y. H. Chu, D. Kan, I. Takeuchi, V. Nagarajan, S. V. Kalinin, *Nat. Commun.* **2012**, *3*, 775.
[39] M. Guennou, P. Bouvier, G. S. Chen, B. Dkhi, R. Haumont, G. Garbarino, J. Kreisel, *Phys. Rev. B* **2011**, *84*, 174107.
[40] M. Guennou, P. Bouvier, R. Haumont, G. Garbarino, J. Kreisel, *Phase Transitions* **2011**, *84*, 474.
[41] R. Haumont, P. Bouvier, A. Pashkin, K. Rabia, S. Frank, B. Dkhil, W. A. Crichton, C. A. Kuntscher, J. Kreisel, *Phys. Rev. B* **2009**, *79*, 184110.
[42] M. D. Peel, S. P. Thompson, A. Daoud-Aladine, S. E. Ashbrook, P. Lightfoot, *Inorg. Chem.* **2012**, *51*, 6876.
[43] Note that such complex AFD structures can also be conveniently analyzed by decomposing the structural distortion, as defined with respect to the reference cubic phase, in terms of symmetry-adapted modes. This can be done by using web-based tools such as ISODISTORT (http://stokes.byu.edu/iso/isodistort.html) or AMPLIMODES (http://www.cryst.ehu.es/cryst/amplimodes.html). Typically, such an analysis will reveal that the distortions are associated to two families of *k*-points corresponding to the Brillouin zone of the 5-atom cubic cell, namely, (0,0,k_z) and (1/2,1/2,k_z), where the z direction is chosen to lie along the complex-tilting pattern. Then, the main periods associated to a particular structure will be given by the values of k_z corresponding to the modes with the greatest contribution to the distortion. This is in essence the approach we adopted to analyze the results of our effective-Hamiltonian simulations (see, e.g., Figure 1c and 1d) (last accessed May, 2012).
[44] J. B. Neaton, C. Ederer, U. V. Waghmare, N. A. Spaldin, K. M. Rabe, *Phys. Rev. B* **2005**, *71*, 014113.
[45] P. Fischer, M. Polomska, I. Sosnowska, M. Szymanski, *J. Phys. C* **1980**, *13*, 1931.
[46] J. P. Perdew, K. Burke, M. Ernzerhof, *Phys. Rev. Lett.* **1996**, *77*, 3865.
[47] a) G. Kresse, J. Furthmuller, *Phys. Rev. B* **1996**, *54*, 11169; b) G. Kresse, D. Joubert, *Phys. Rev. B* **1999**, *59*, 1758.
[48] P. E. Blöchl, *Phys. Rev. B* **1994**, *50*, 17953.